
**Aerosol Science and Technology**
Publication details, including instructions for authors and subscription information:
http://www.informaworld.com/smpp/title~content=t713656376

# Surface-Contact Mechanics During Oblique Impact of Microspheres with Planar Surfaces

Patrick F. Dunn [a]; Raymond M. Brach [a];Gregory G. Janson [a]
[a] PARTICLE DYNAMICS LABORATORY, DEPARTMENT OF AEROSPACE AND MECHANICAL ENGINEERING, UNIVERSITY OF NOTRE DAME, NOTRE DAME, IN

First published on: 01 January 1996

**To cite this Article** Dunn, Patrick F. , Brach, Raymond M. andJanson, Gregory G.(1996) 'Surface-Contact Mechanics During Oblique Impact of Microspheres with Planar Surfaces', Aerosol Science and Technology, 25: 4, 445 — 465, First published on: 01 January 1996 (iFirst)
**To link to this Article: DOI:** 10.1080/02786829608965409
**URL:** http://dx.doi.org/10.1080/02786829608965409

# Surface-Contact Mechanics During Oblique Impact of Microspheres with Planar Surfaces

*Patrick F. Dunn,* Raymond M. Brach, and Gregory G. Janson*
PARTICLE DYNAMICS LABORATORY,
DEPARTMENT OF AEROSPACE AND MECHANICAL ENGINEERING,
UNIVERSITY OF NOTRE DAME, NOTRE DAME, IN 46556

**ABSTRACT.** The surface-contact mechanics and impact characteristics of a microsphere with an inclined planar surface are examined by experiments and numerical simulation. The results of base-case experiments are presented in which monodisperse, electrically neutral microspheres obliquely impact a molecular-smooth flat surface under vacuum. Experiments different from the base case delineate the effects of variations in surface material properties and roughness, and microsphere material properties, size, spin and electrical charge. The presence of microsphere spin prior to impact is found to significantly affect the impact response. The nature of the contact mechanics changes and is affected by variations in surface and microsphere material properties. Increased surface roughness alters the microsphere's impact response and biases experimental results at shallow incidence angles, at times yielding apparent coefficients of restitution greater than unity. Finally, electrical charge is shown to lower the microsphere's rebound velocity most appreciably at normal incidence.  AEROSOL SCIENCE AND TECHNOLOGY 25:445–465 (1996)



## INTRODUCTION

The impact of a particle with a surface continues to receive considerable attention in the scientific and technical communities primarily because of this problem's fundamental nature, as well as its innumerable applications. Over the past 20 years, attention has been directed toward examining the impact of very small (micrometer-sized) particles with surfaces, where additional forces are present that contribute to particle adhesion. This problem is relevant to many contemporary applications, e.g., spacecraft particulate contamination (Fong et al., 1995) and microelectronics manufacturing (Cooper et al., 1990). The July 1995 special issue of *Aerosol Science and Technology* (vol. 23) on the "Interactions of Particles with Surfaces" presents some of the more recent findings and reviews most of the previous studies in this area. The present paper extends the experimental studies of the oblique impact of a microsphere with a planar surface presented by Dunn et al. (1995), and applies the dynamic simulation model of Brach and Dunn (1995) to the

*To whom correspondence should be addressed.

Aerosol Science and Technology 25:445–465 (1996)

Published by Elsevier Science Inc.

0278-6826/96/$15.00
PII S0278-6826(96)00101-8

new experimental results reported herein. Particular emphasis is placed on elucidating the effects of incidence angle, the microsphere's initial angular velocity, and surface roughness on the surface-contact mechanics and rebound characteristics.

Various models have been proposed for the normal and oblique impact of a microsphere with a planar surface (*Aerosol Science and Technology*, July 1995). Many have contributed to our understanding of the physics of the impact problem. Each model has required some experimental information to "calibrate" the model before subsequent predictions can be compared with experiments. One objective of the present study is to obtain further, detailed experimental information on the surface-contact mechanics. This should lead to improving the models and reducing the required *a priori* information.

There are very few experimental studies of the oblique impact of microspheres with flat surfaces (*Aerosol Science and Technology*, July 1995). The oblique impact of nonspherical, micrometer-sized particles has been investigated, such as pollen and spores onto cylinders and stems (Aylor and Ferrandino, 1985) and onto leaf surfaces (Paw U, 1983), and fly ash onto metal surfaces (Tabakoff and Malak, 1987). The oblique impact of microspheres has been studied for the cases of glass microspheres impacting the edge of a slowly rotating wheel (Broom, 1979) and an aluminum plate (Buttle et al., 1989), and for ammonium fluorescein microspheres impacting a stainless steel cylinder (Wang and John, 1988). Several findings from these experiments pertain to the present study.

The experiments of Broom (1979), Aylor and Ferrandino (1985), and Wang and John (1988) all support a hypothesis that the microparticle's tangential and normal velocity components both influence the process of microparticle capture by or rebound from the surface. Both Aylor and Ferrandino (1985) and Broom (1979) show that adhesion and rebound are related directly to the total (absolute) velocity of impact. Wang and John (1988) provide experimental evidence that for oblique impacts at small incidence angles, rebound can occur when the incident normal velocity component is less than the critical normal capture velocity.

The studies of Aylor and Ferrandino (1985), Buttle et al. (1989), and Wang and John (1988) further demonstrate that the coefficient of restitution based upon the normal velocity components varies with incidence angle, and suggest that this variation possibly is related to effects such as surface roughness or particle spin. Aylor and Ferrandino (1985) argue that the coefficient of restitution may not be constant, but may increase as the incidence angle becomes more oblique. Buttle et al. (1989) attribute an observed increase in the value of the coefficient of restitution (from 0.51 at 90° [normal] and 50° incidence to 0.68 at 29° incidence) to "a reduction in the frictional force ... at large angles," the rotation of the particle, or possibly plastic deformation during impact. Broom (1979) mentions that the roughness of the impact surface is also important, where more polished surfaces might exhibit a higher value of the coefficient of restitution for all angles of incidence. He refers to the study of Lifshitz and Kolsky (1964) on the normal impact of large (mm-sized) spheres onto surfaces, where the value of the coefficient increased from 0.82 to 0.95 as the surface was more finely polished. Wang and John (1988) argue how a surface protrusion (a roughness) at low incidence angles effectively increases the angle of incidence, and thus the inbound normal velocity component to a value greater than the critical normal capture velocity, thereby yielding particle rebound.

The present work examines the rebound characteristics of a microsphere from a planar surface as the angle of incidence is changed. It also examines the effects of several parameters that affect the oblique impact process. These include surface material properties and roughness, and microsphere material properties, size, spin, and electrical charge. The experimental approach taken in this study was to first establish a "base case" in which these parame-

ters were controlled or minimized. This was done by using relatively monodisperse, electrically neutral microspheres impacting a molecular-smooth planar surface under vacuum. Then, additional experiments were performed in which these parameters were systematically varied. In this manner, the sensitivity of the microsphere's rebound characteristics to particular parameter variations was determined and the physical reasons for the observed variations explained.

The following presents the results of these experiments during which measurements were acquired for *individual* oblique impact events (i.e., the incident and rebound velocity components were measured *for the same microsphere*). These results are likely the first of their kind to be reported in the open literature. Most of the experimental equipment and approach used here was first described by Caylor et al. (1992). An analysis is presented to show approximately how surface roughness can bias the measured values of the rebound angle and the impact coefficients (restitution and impulse ratio) at shallow angles of incidence. Finally, comparisons of the experimental results with an impact simulation are given.

## EXPERIMENTAL SYSTEM AND APPROACH

The experimental system developed by Caylor (see Dunn et al., 1995) to investigate the impact of microspheres with planar surfaces under vacuum conditions ($\sim 10^{-4}$ torr) was used in the present study. A schematic of the system is shown in Fig. 1. In the subject experiments, various microspheres were ejected from a dispenser and accelerated vertically downward by gravity to the target surface. The microspheres were dispensed using either an electrostatic particle dispenser (EPD) or a neutral particle dispenser (NPD) operated in tandem with the EPD. The exit of either dispenser

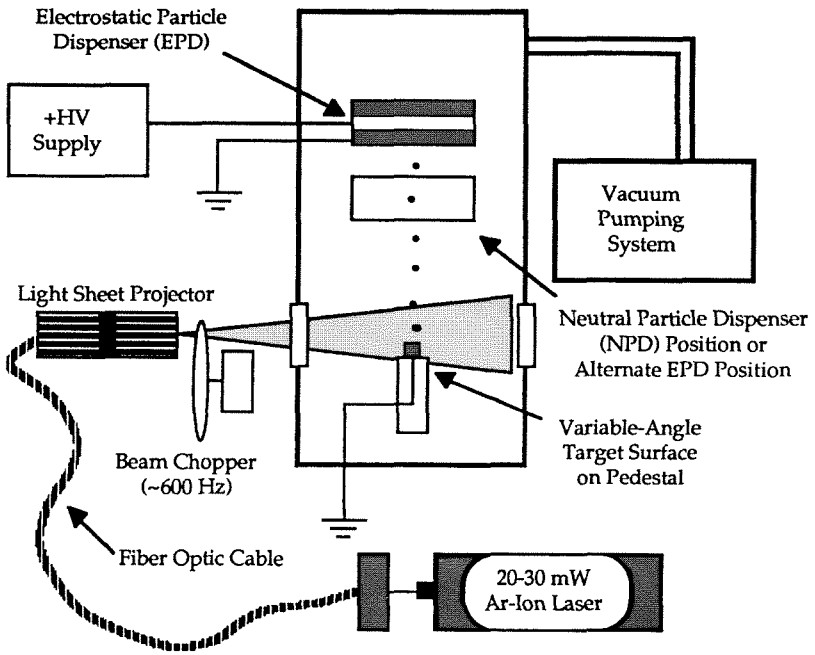


FIGURE 1. Schematic of the experimental configuration.

was either 14 or 21 cm above the target surface, yielding microsphere velocities from ~1.7 to 2.0 m/s upon normal (90°) incidence impact with the surface. A target surface was oriented at angles ranging from ~10° to 90° with respect to vertical such that either normal or oblique impacts could be studied. A particle trajectory imaging system (PTIS) employing a pulsed laser light sheet visualization technique in conjunction with a video analysis system was used to determine the particle incident and rebound, normal, and tangential velocity components. The reader is referred to Caylor et al. (1992) and Caylor (1993) for a detailed description of the components of this experimental system, and to Janson (1995) for a further description of recent modifications to Caylor's system. Additional information pertinent to the present experiments follows.

### *Particles and Impact Surfaces*

Eight surface and four particle materials were used in the present study. Six of the 15 particle/surface combinations studied are presented herein. These cases adequately illustrate the effects of microsphere spin, material properties, and surface roughness on the rebound characteristics of the microsphere. The reader is referred to Janson (1995) for more comprehensive results.

The experimental conditions for these six combinations are given in Table 1. Case 1 represents the "base case" of this study, in which electrically neutral, relatively monodisperse microspheres and a molecular smooth surface were used. Variations in conditions from this case allowed the various effects to be evaluated. For case 2, a different particle dispenser was used to assess the effects of microsphere spin (as compared to case 1). Case 3 conditions were similar to case 1, except that a relatively rough surface was used. The differences between cases 4 and 5 show the effects of different surface material roughness and microsphere/surface stiffness. A comparison between cases 5 and 6 illustrates the effects of differences in microsphere size and material properties.

The characteristics and material properties of the 10–65 $\mu$m diameter stainless steel and the 1–30 $\mu$m diameter Ag-coated glass microspheres and the aluminum and Tedlar™ surfaces are presented in Dunn et al. (1995). The material properties of the 64–76 $\mu$m diameter stainless steel microspheres were similar to the 10–65 $\mu$m diameter ones, but with a number-weighted mean diameter ($d_{10}$) of 70 $\mu$m.

The $SiO_2$-coated and the uncoated silicon wafer surfaces were prepared specifically for this study. The material properties of the these surfaces were that of single crystal (1,0,0) silicon. The $SiO_2$ coating on

**TABLE 1. Conditions of Particle/Surface Combinations for Experiments**

| | Microsphere | | | | Surface | | | | | |
|---|---|---|---|---|---|---|---|---|---|---|
| Case | $d_{10}$ | $\rho$ | $\nu$ | $E$ | Material | $\rho$ | $\nu$ | $E$ | $k$ | $d^*$ |
| 1 | 70 | 8000 | 0.27 | 190 | $Si/SiO_2$ | 2330 | 0.28 | 130 | 110 | 15500 |
| 2 | 70 | 8000 | 0.27 | 190 | Si | 2330 | 0.28 | 130 | 110 | 68 |
| 3 | 70 | 8000 | 0.27 | 190 | Si | 2330 | 0.28 | 130 | 110 | 68 |
| 4 | 50 | 8000 | 0.27 | 190 | aluminum | 2700 | 0.33 | 69 | 75 | 1000 |
| 5 | 50 | 8000 | 0.27 | 190 | Tedlar™ | 1460 | 0.33 | 2.1 | 3.1 | 125 |
| 6 | 8.6 | 2600 | 0.21 | 72 | Tedlar™ | 1460 | 0.33 | 2.1 | 3.1 | 20 |

Note: Microsphere material was stainless steel for cases 1–5; Ag-coated glass for case 6. NPD used for cases 1, 3; EPD used for cases 2, 4–6.
$d_{10}$ ($\mu$m): number-weighted mean diameter.
$\rho$ (kg/m$^3$): density.
$\nu$: Poisson's ratio.
E(GPa): Young's modulus.
k(GPa): Hertzian stiffness.
$d^*$: $d_{10}$/maximum asperity height.

the wafer was grown using thermal oxidation procedures (Sze, 1983; Ghandhi, 1983). An ellipsometer showed the coating on the surface to be approximately 500 nm thick. The surfaces were cut to approximately scanning electron microscope (SEM) mount size using a diamond-tipped etching tool such that they could be mounted in the test cell. The substrate was attached to an SEM mount using high-purity silver paste. Each surface was used for only one experiment. Narrow-range profilometer plots of the two surfaces are presented in Fig. 2, showing a maximum vertical variation of only 45 Å for

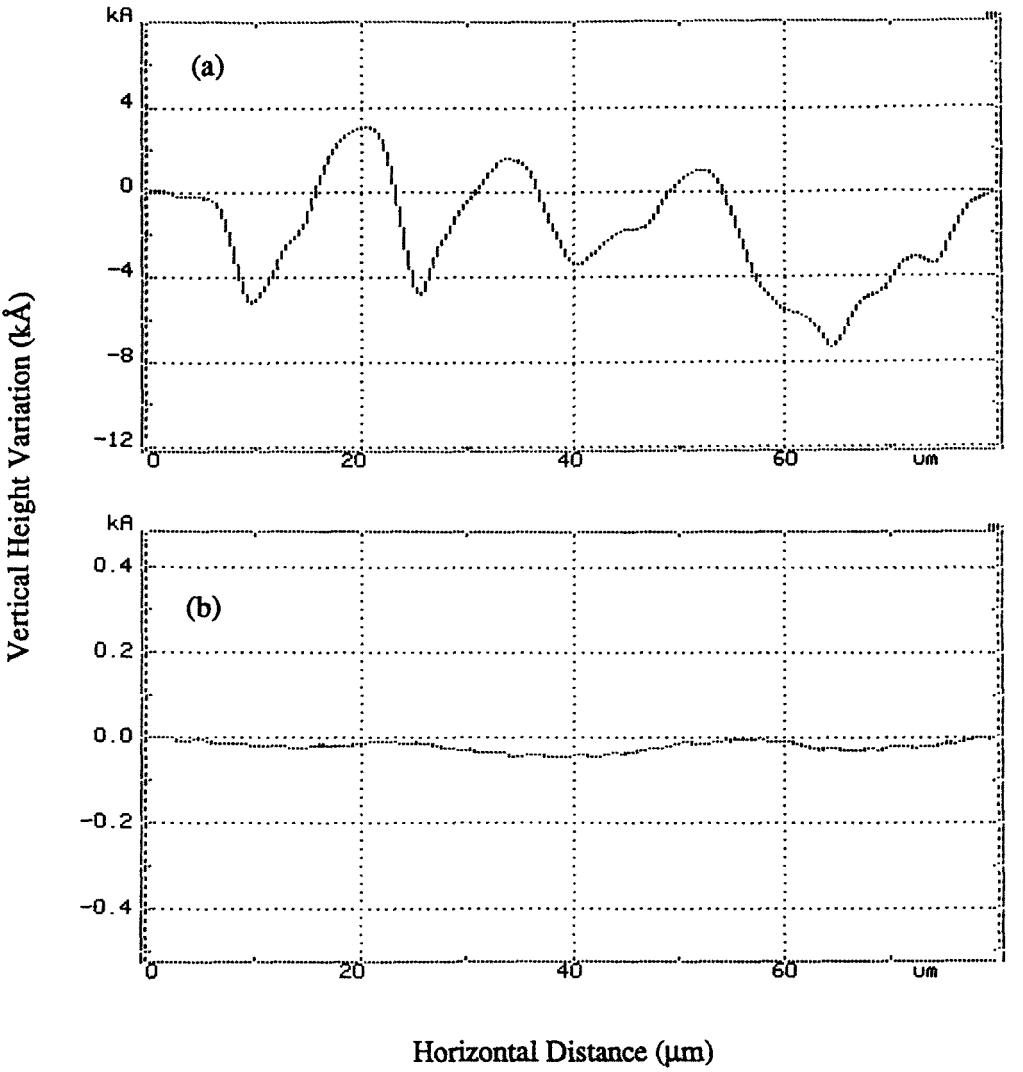


FIGURE 2. Narrow-range profilometer plots of substrate surfaces: (a) uncoated substrate, (b) $SiO_2$-coated substrate (note the difference between the horizontal and vertical scales). Note: 1 kÅ = 0.1 $\mu$m.

the coated surface and ~200 times greater for the uncoated surface over a horizontal range of 80 $\mu$m.

The "roughness" for each microsphere/surface combination was characterized by $d^*$, the ratio of the microsphere's number-weighted mean diameter ($d_{10}$) to the maximum asperity height of the surface. The asperity heights were measured directly using a profilometer for cases 1, 2, and 3, and were estimated from scanning electron micrographs for cases 4, 5, and 6. The values of $d^*$ are presented in Table 1.

### *Measurement Uncertainties*

An uncertainty analysis at the 95% confidence level (Coleman and Steele, 1989) was performed to estimate the uncertainties in the measured values of the microsphere's velocity components and impact angles, and in the resulting computed values of the coefficients of restitution and the impulse ratios. Refer to Janson (1995) for details.

The configuration and coordinate system for microsphere impact with a planar surface is illustrated in Fig. 3. The microsphere's incident velocity vector **v** has normal and tangential components $v_n$ and $v_t$, respectively. The angle of incidence with respect to the surface is $\alpha_i$ (normal incidence $\Rightarrow \alpha_i = 90°$), the microsphere's initial angular velocity is $\omega$, and its initial surface velocity (relative to its center of mass) is $r\omega$. The microsphere's rebound velocity **V** has components $V_n$ and $V_t$. Its rebound angle is $\alpha_r$ and its final angular velocity is $\Omega$. The definitions of the coefficient of restitution $e$ and the impulse ratio $\mu$ can be written in terms of the velocity components, where $e = -V_n/v_n$ and $\mu = (V_t - v_t)/(V_n - v_n)$. The latter is the ratio of the total impulse of the tangential surface force to the total impulse of the normal contact forces.

The uncertainties for the normal and tangential velocity components and the incidence angles arise from uncertainties in measuring distances and angles as recorded on the digitized video images of the PTIS, and from uncertainty in the strobe frequency. These vary over the incidence angle range, and combine to yield measurement uncertainties in the normal and tangential, incident, and rebound velocity components. A calibration experiment of the digitization software resulted in an angle uncertainty (95%) of $\pm 0.35°$ and in a length scale uncertainty (95%) of $\pm 3.1\%$. The resolution of the stroboscope is $\pm 0.5$ Hz. Over the incidence angle range from 10° to 90°, the normal velocity component measurement uncertainties decrease from $\pm 5\%$ to $\pm 3\%$, and the tangential velocity component measurement uncertainties increase from $\pm 3\%$ to $\pm 4\%$. The resulting measurement uncertainties in the coefficient of restitution and the impulse ratio are less than $\pm 10\%$ over the same range.

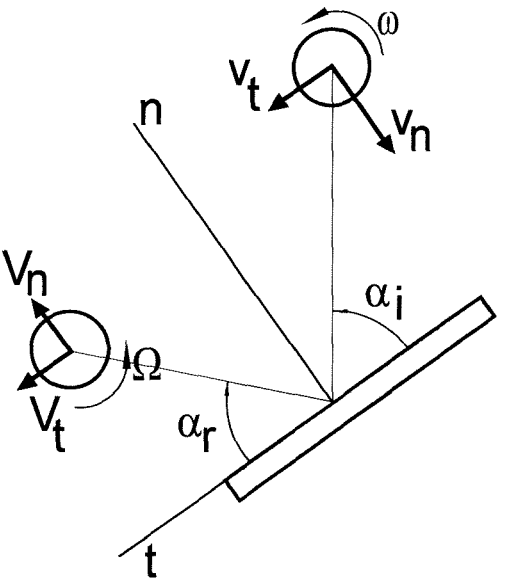


FIGURE 3. Impact coordinates and notation.

In the following presentation of the experimental results, the sample mean value of a quantity is plotted with error bars. Each error bar region denotes the region within which the quantity's true mean value is estimated to be with 95% confidence. The extent of this region was determined from a standard uncertainty analysis at the

95% confidence level, in which the measurement uncertainty (the "measurement bias limit") and the finite sampling uncertainty (the "measurement precision index") were combined in quadrature to yield the overall measurement uncertainty of that quantity.

Also, the sample mean value of each quantity is determined by first computing the quantity's value for *each* impact event (from the incident and rebound velocity components measured *for the same particle*), and then subsequently its mean value for the ensemble of particles is considered. This approach contrasts that in which the average incident and rebound velocity component values are each computed first for the ensemble of particles, and then used to determine the quantity's mean value. The latter approach results in a bias error for the true mean value estimate whenever the quantity of interest involves products or quotients of measured quantities that are ensemble-averaged first.



## RESULTS AND DISCUSSION

### *Base-Case Results*

The sample mean values of the impulse ratio ($\mu$), coefficient of restitution ($e$), and rebound angle ($\alpha_r$) are plotted in Fig. 4 versus the incidence angle ($\alpha_i$) for the base case. As displayed by the top graph in this figure, the average impulse ratio value begins from an approximate zero value at $\alpha_i = 90°$ and then increases with decreasing incidence angle. From $\alpha_i = \sim 45°$ down to $\sim 20°$, the value of $\mu$ is constant to within the measurement uncertainty. Below $\alpha_i = \sim 20°$, the value of $\mu$ decreases. As described by Brach and Dunn (1995) and in further detail by Janson (1995), this behavior signifies four incidence angle regions in which the mechanics of contact are distinctly different. Each of these regions (I–IV) are denoted in the figure. In region I, the microspheres are rolling by the end of surface contact. In region III, the microspheres slide throughout contact, where the constant impulse ratio value is the friction coefficient $f$. Region II is a transition region in which some of the microspheres slide throughout contact and some are rolling by the end of contact. Region IV is characterized by a decreased tangential impulse.

The figure also shows the critical impulse ratio ($\mu_c$) curve denoted by $r\omega = 0$. It is calculated from the rigid body impact theory of Brach and Dunn (1995) for the conditions of rolling at the end of contact. It can be shown that

$$\mu = \mu_c = \left(\frac{1}{1+\lambda}\right)\left(\frac{1}{1+e}\right)\eta \qquad (1)$$

in which $\eta = (v_t - r\omega)/v_n$, $\lambda = r^2/k^2$ and $k$ is the centroidal radius of gyration. For a sphere, $\lambda = 5/2$ and for a point mass, $\lambda = 0$. For $\omega = 0$, $\eta = 1/\tan\alpha_i$ where $\tan\alpha_i = -v_n/v_t$. The dashed impulse ratio curve shown in Fig. 4 is from Eq. (1) for a sphere. Departure of the data from this curve as the incidence angle is decreased earmarks the transition region (II).[1] This theoretical relation among $\mu_c$, $e$, and $\alpha_i$ shows how tangential and normal effects behave in region I, and demonstrates close agreement between the data and the theory.

The middle graph in the figure reveals that over the incidence angle range from $\sim 45°$ to 90°, the coefficient of restitution is constant to within its true mean value estimates. This corresponds to normal velocity component ($v_n$) values from 1.25 to 2.25 m/s (recall $v_n = v \sin\alpha_i$). The trend of a relatively constant value of $e$ over an incident normal velocity range has been reported for the case of normal incidence (see Fig. 6 in Brach and Dunn (1995), for example). This trend signifies where adhesion begins to affect microsphere rebound. For incidence angles below $\sim 45°$($v_n < \sim 1.25$ m/s), the coefficient of restitution values decreases with decreasing incidence angle, illustrating more pronounced adhesion

[1]This implicitly assumes that the true mean initial rotational velocity of the microspheres is zero, which is valid to within the measurement uncertainty for the present experiments.

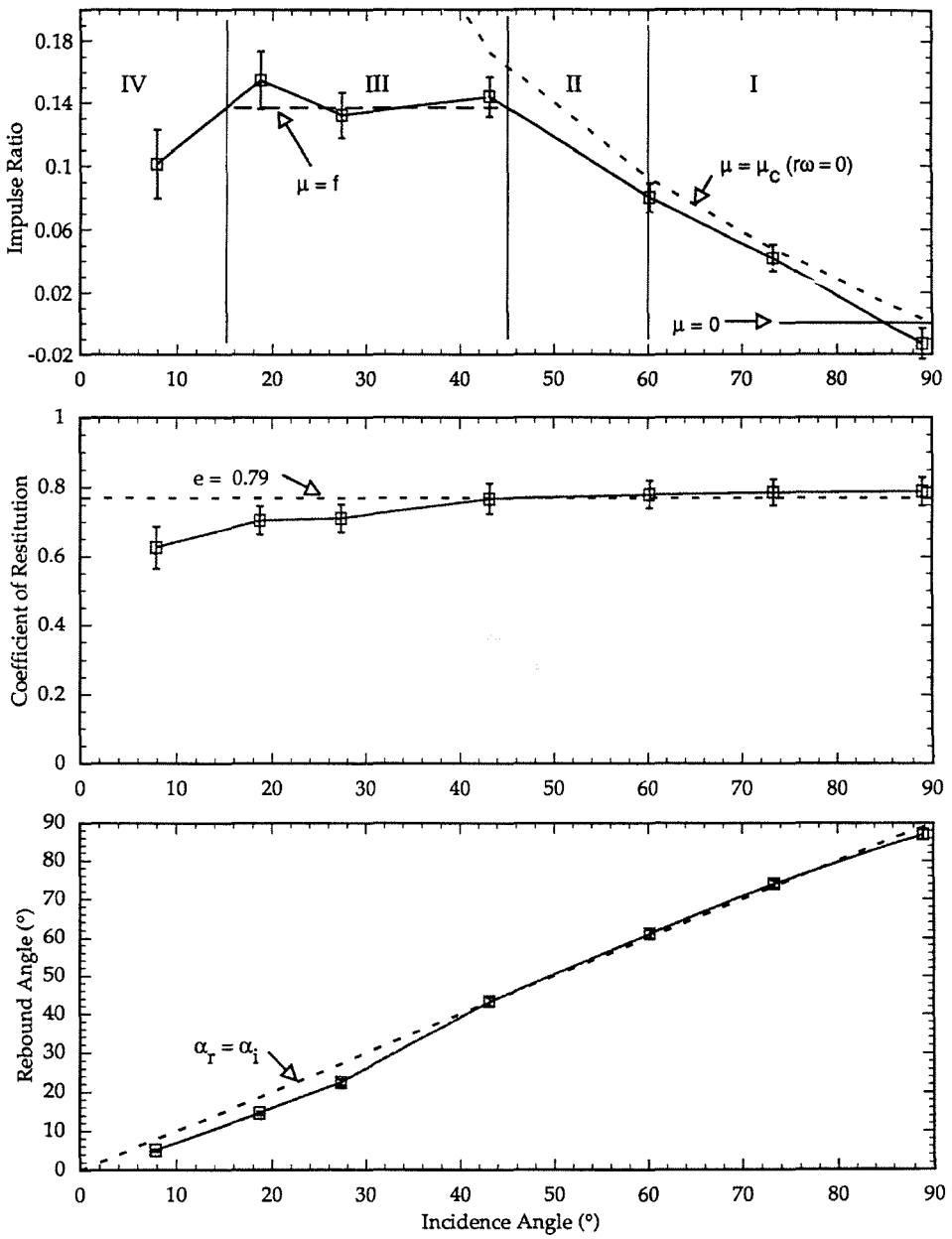


FIGURE 4. Impulse ratio, coefficient of restitution and rebound angle versus incidence angle: case 1.

effects. No microsphere capture was observed down to the lowest $v_n$ examined (0.25 m/s).

As displayed by the bottom graph in the figure, over the incidence angle range from ~45° to 90°, the rebound angle equals the incidence angle, as evidenced by the line $\alpha_r = \alpha_i$ passing through the data to within the overall measurement uncertainty. Over this incidence angle range, the microsphere is reflected *specularly* from the surface. The relation between $\alpha_i$ and $\alpha_r$ for the entire incidence angle range is

$$\tan \alpha_r = \frac{e \tan \alpha_i}{1 + \mu(1+e)\tan \alpha_i}. \quad (2)$$

Assuming $\mu = \mu_c$ and $\omega = 0$ and using Eq. (2), it can be shown that

$$\tan \alpha_r = (7/5)e \tan \alpha_i. \quad (3)$$

Thus, for the range of incidence angles over which $e$ is constant and approximately equal to 5/7, Eq. (3) reduces to $\alpha_r \approx \alpha_i$. For incidence angles below ~45°, the microsphere is not reflected specularly, but at an angle less than the incidence angle. From Eq. (2), this appears to result from lower values in $e$ over this incident angle range, where $\mu(1+e)\tan \alpha_i \ll 1$.

Another important quantity is the kinetic energy loss due to impact. The angular velocities of the microspheres currently are not measurable, so the experimental energy loss must be computed from the change in translational velocity only. The normalized kinetic energy loss $T_L^*$ is defined as the initial kinetic energy minus the final kinetic energy, all divided by the initial. For experimental results, this is $T_L^* = (v^2 - V^2)/v^2$, where $v^2 = v_n^2 + v_t^2$ and $V^2 = V_n^2 + V_t^2$. In general, for an impact of any rigid body, $T_L^*$ can be related to the angle of incidence, coefficient of restitution, and impulse ratio (Brach, 1991) as

$$T_L^* = [1 - e^2]\sin^2\alpha_i + (\mu/\mu_c)[2 - (\mu/\mu_c)]\cos^2\alpha_i. \quad (4)$$

Figure 5 shows the base-case energy loss data and Eq. (4) plotted (dashed curve) with $\mu_c$ from Eq. (1) for a point mass ($\lambda = 0$) and for the nominal values of $e = 0.79$ and $f = 0.14$. The experimental results agree to within measurement uncertainty with the theoretical $T_L^*$ (dashed) curve for point masses except at two intermediate incident angles ($\alpha = \sim 60°$ and $\sim 74°$). Whether or not it is justifiable to ignore rotational kinetic energy in this comparison will be considered further in subsequent sections.

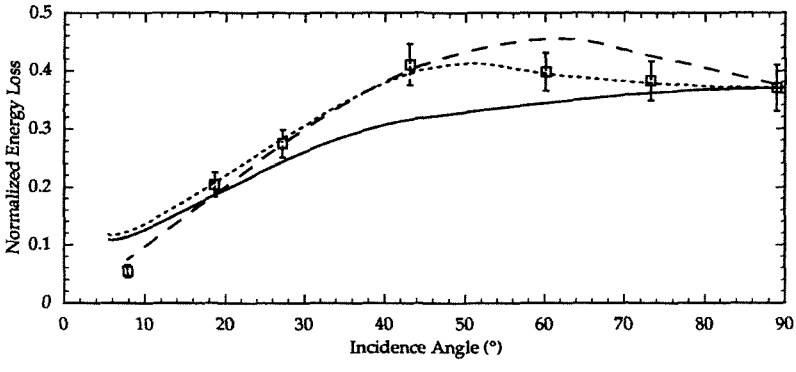


FIGURE 5. Normalized translational kinetic energy loss versus incidence angle: case 1. Eq. (4) (dashed curve); simulation including rotational energy (solid curve); simulation excluding rotational energy (dotted curve).

### *Rotational Effects*

The experimental conditions established for the base case permit estimation of the microsphere's initial angular velocity $\omega$. This is done by assuming that the only factor contributing to a nonnormal rebound angle from a flat surface *for normal incidence* is the microsphere's initial spin. Under the assumption of rolling at separation, Brach and Dunn (1995) show that $r\omega = (7V_t - 5v_t)/2$. The final tangential velocity component data acquired in region I then can be used to determine $\omega$ for a given value of the microsphere radius.

The resulting frequency distribution of the microspheres' initial surface velocities determined for the $\alpha_i \sim 90°$ base case is presented in Fig. 6, labeled "NPD." Here, the microspheres' incident (initial) surface velocities due to spin range from $r\omega = -0.64$ m/s to $r\omega = 0.62$ m/s ($\Delta r\omega = 1.26$ m/s). This corresponds to a range of incident angular velocities from $-1.8 \times 10^4$ to $1.8 \times 10^4$ rad/s for a microsphere radius of 35 $\mu$m. This distribution is not symmetric about a mean value of $r\omega = 0$. This contributes to a bias in the experimentally measured value of $\mu$ (see the top graph in Fig. 4 for $\alpha_i = 90°$).

Microspheres dispensed by the EPD are expected to have higher incident angular velocities as a result of the large number of microsphere/wall collisions within the dis-

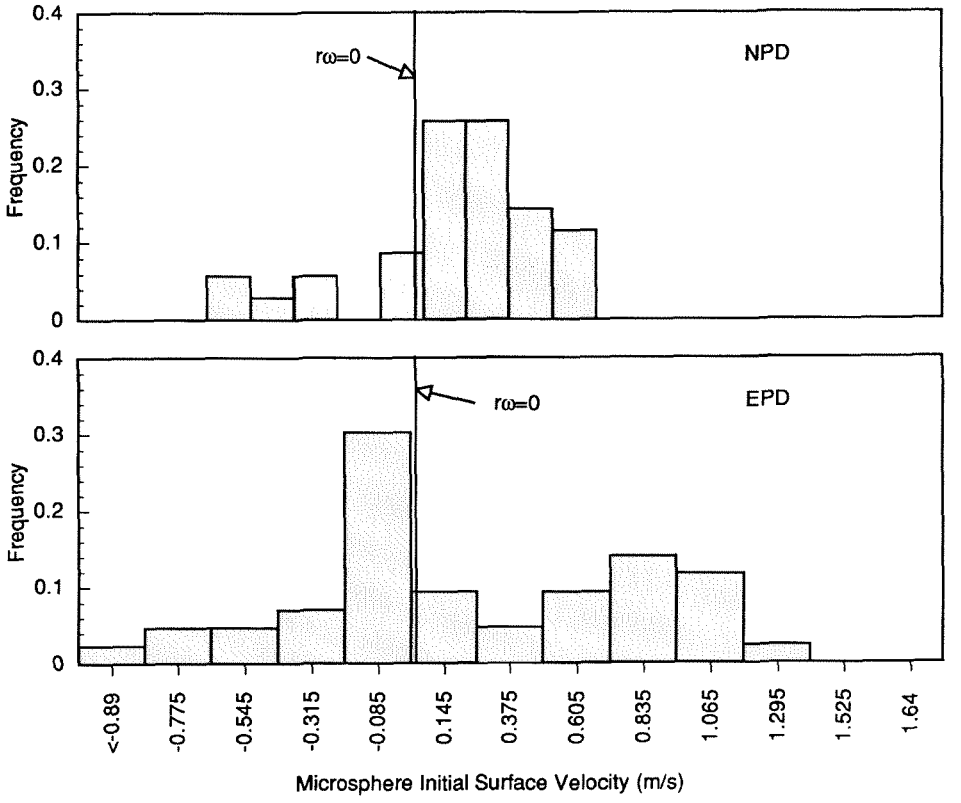


FIGURE 6. Frequency distribution of microsphere initial surface velocity at $\alpha_i = 90°$: (a) case 1, NPD-dispensed microspheres, (b) case 2, EPD-dispensed microspheres.

penser and the slope of its walls. In Fig. 6 for the frequency distribution labeled "EPD," the incident tangential velocity range is seen to extend from $-0.89$ to 1.33 m/s (or $\Delta r\omega = 2.22$ m/s). This corresponds to a range of incident angular velocities from $-2.5 \times 10^4$ to $3.8 \times 10^4$ rad/s for a microsphere radius of 35 $\mu$m. This approximate doubling in the incident angular velocity of microspheres dispensed by the EPD versus the NPD results in increases in the ranges of $\alpha_r$ (from $\Delta\alpha_r = 7.7°$ to $\Delta\alpha_r = 30.6°$) and $\mu$ (from $\Delta\mu = 0.116$ to $\Delta\mu = 0.223$), and a slight decrease in the range of $e$ (from $\Delta e = 0.31$ to $\Delta e = 0.26$). These data and the above analysis indicate that the initial angular velocities of microspheres under these experimental conditions can be large and affect the impact process significantly.

### *Surface Roughness Effects*

In general, variations in physical conditions can introduce both variability and bias in experimental measurements. Surface roughness can cause a local normal at the contact area to differ from an ideal or nominal surface normal, and thereby influence the values of the $e$s and $\mu$s calculated from the data. Random surface irregularities can cause biases for shallow (low $\alpha_i$) oblique impacts because of a "shadow zone" behind wave peaks, such as seen in Fig. 2a. Consider a planar view of a wavy surface at a point where the local normal makes a clockwise angle $\phi$ to the nominal and where the counterclockwise angle of incidence from the nominal tangential axis is $\alpha_i$, as illustrated in Fig. 7. The incident and rebound angles of a microsphere are observed and measured relative to the nominal surface, whereas $e$ and $\mu$ should be calculated from velocity component measured relative to the true local tangent and normal. For relatively small surface waviness, the assumptions $\sin\phi \approx \phi$ and $\cos\phi \approx 1$ can be made. When $\alpha_i$ is also small, the measured values $e_m$ and $\mu_m$ of the coefficients can be shown to be

$$e_m \approx \left[1 + \frac{\phi}{\alpha_i}\right]\left[e + \frac{\phi}{\alpha_i + \phi}\right] \tag{5}$$

and

$$\mu_m = \mu - \phi \tag{6}$$

where $\mu = \pm f$ for sliding throughout contact. Because a microsphere approaching a wavy surface at shallow angles is less likely to hit a backside of a protuberance, $\phi$ is more likely to be positive and $e_m$ is more likely to be larger than the true value $e$. Note that for $\phi \approx \alpha_i$, $e_m$ can exceed $2e$. The impulse ratio can be positive or negative, depending on the sign convention and sign of $v_t$. For the $\phi$ illustrated in Fig. 7, $\mu = -f$, and so the computed impulse ratio

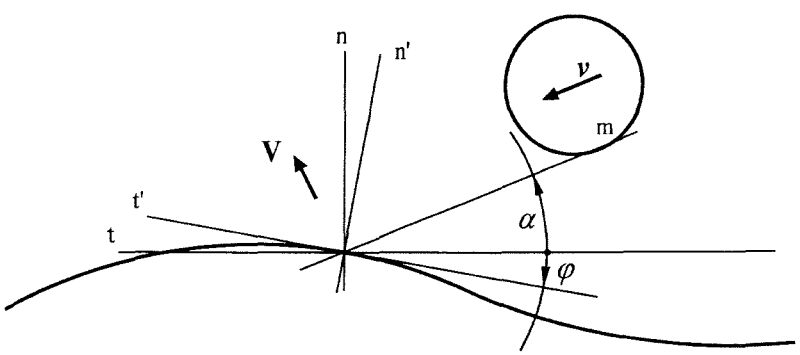


FIGURE 7. Geometry and coordinates for surface roughness analysis.

will have a magnitude larger than the true one. Finally, if the true rebound angle equals the true incidence angle, a measured rebound angle greater than its true value will result because the true incidence angle equals $\alpha_i + \phi$. Thus, these equations imply that for small angles of incidence, the rebound angles and restitution coefficients are larger than their true values and the impulse ratios are larger in magnitude than their true values.

Corresponding data are illustrated in Fig. 8. The top graph of $\alpha_r$ versus $\alpha_i$ reveals that the effect of surface roughness is to increase $\alpha_r$ at a given $\alpha_i$. The middle and bottom graphs show that surface roughness manifests itself as an increase in $e$ (from 0.63 to 1.22) and in the magnitude of $\mu$ (from 0.10 to 0.15) for a fixed $\alpha_i$ (7.9) from their "smooth" surface values. The value of $e$ increases to greater than unity; this should not be surprising in light of the above observation from Eq. (5) that $e_m$ can exceed $2e$. Using the average value of $\phi$ obtained from a profilometer plot of the "rough" surface (2.42°) and the true values of $e$ and $\mu$ from the "smooth" surface case, Eqs. (5) and (6) can be used to predict measured values of $e_m$ and $\mu_m$. The predicted values of $e_m = 1.22$ and $\mu_m = 0.14$ match the experimental values almost exactly. Values of $e$ greater than unity have been reported in other experiments involving the oblique ($\alpha_i = 17.5°$) impact of glass microspheres ($\sim$ 190 $\mu$m in diameter) with a glass plate (Shaffer et al., 1994).

At near-normal incidence, the effects of surface roughness differ. Consider $\alpha_i$ nearly perpendicular to the nominal surface and $\omega = 0$. Analysis shows that a small local slope $\phi$ gives a measured coefficient $e_m = e - (9/7)\phi^2$. Measured values of $e$ therefore will be smaller than the true value. This is observed in the present experiments, where $e_m$ for the rough surface (0.67) is less than that for the smooth surface (0.79) at the same incident normal velocity (1.75 m/s). Similar effects for the normal impact of mm-sized spheres onto surfaces polished to various degrees have been reported by Lifshitz and Kolsky (1964). Analysis also shows that the true impulse ratio is proportional to the negative value of $\phi$, so the impulse ratio will have a nonzero value opposite in sign to the slope of the local tangent. There also can be other contributing factors to nonzero values of $\mu$ at normal incidence, such as an asymmetric distribution of the microspheres' initial surface velocities with a nonzero mean value, as shown previously.

An observed effect at normal incidence of increasing surface roughness is a broadening of the microsphere's rebound angle from the surface. This is seen by comparing the frequency distributions of the rebound angles measured for $\alpha_i \sim 90°$ for the $SiO_2$-coated, "smooth" surface wafer base case and the noncoated, "rough" surface wafer case. These are shown in Fig. 9. The "rough" surface produces a rebound angle range ($\Delta\alpha_r = 25.8°$) broader than the "smooth" surface ($\Delta\alpha_r = 14.1°$). This increase in the range of $\alpha_r$ also leads to an increase in the range of $\mu$ (from $\Delta\mu = 0.116$ to $\Delta\mu = 0.186$), but to no change in the range of $e$ ($\Delta e = 0.31$).

### *Combined Surface Roughness and Material Effects*

The effect of a concomitant change in surface roughness and material can be seen by examining the results of cases 4 and 5 in which the particle type (10–65 $\mu$m diameter stainless steel) was fixed and the type of surface was varied. The two surfaces used were aluminum and Tedlar™, in order of increasing surface roughness and decreasing Hertzian stiffness (see Table 1). The results of the measurements of the rebound angle, coefficient of restitution, and impulse ratio are plotted in Fig. 10 versus the incidence angle for each of the two cases. The top graph reveals that this combined effect manifests itself primarily at low incidence angles (for $\alpha_i \leq \sim 30°$). As $\alpha_i$ is decreased to low incidence angles, the true mean value estimate of $\alpha_r$ for the Tedlar™ surface case departs from its approximate linear relation with $\alpha_i$ and asymptotically approaches a value of $\alpha_r = \sim 16°$. This trend

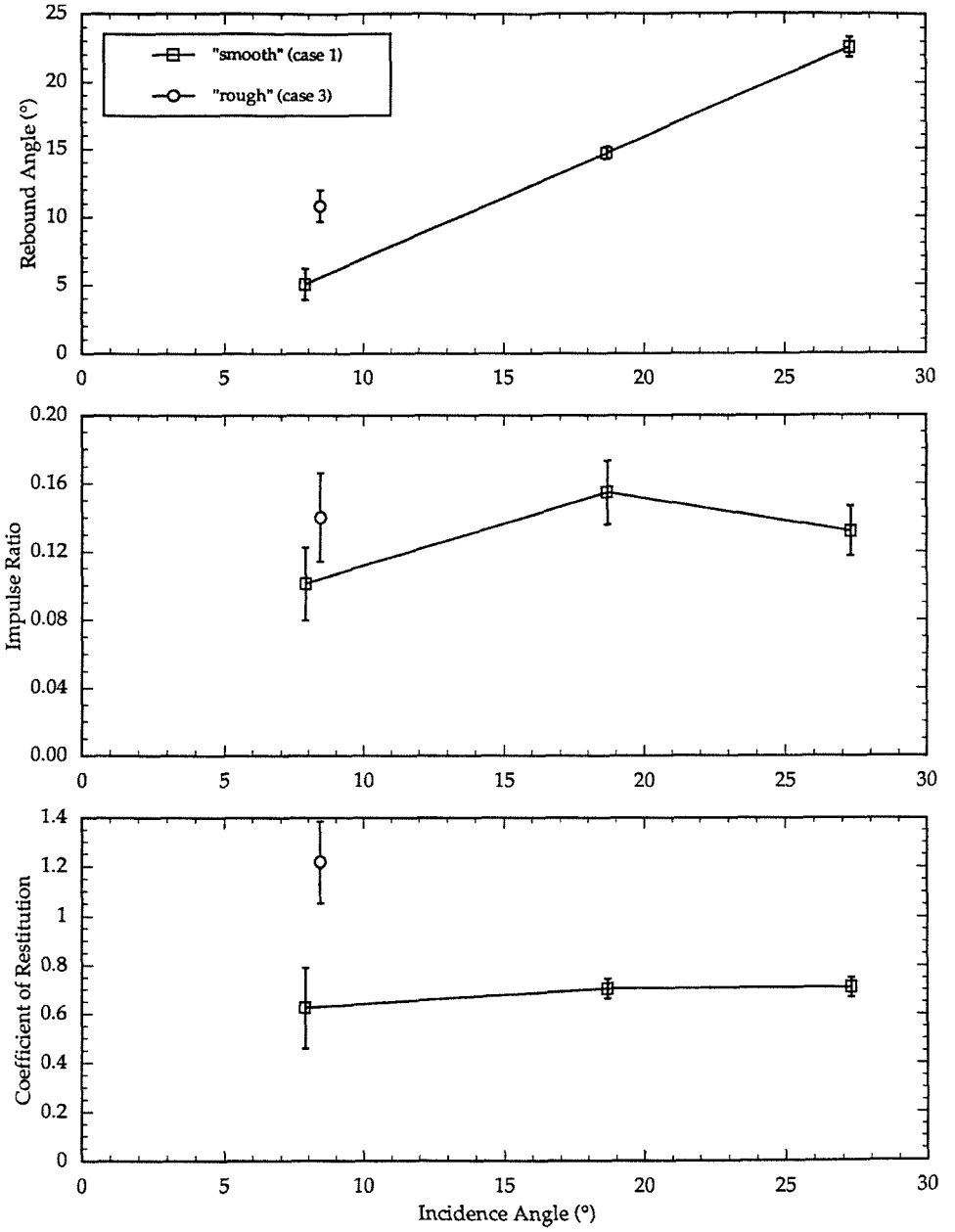


FIGURE 8. Impulse ratio, coefficient of restitution, and rebound angle versus incidence angle: comparison of "smooth" (case 1) and "rough" (case 3) surfaces.

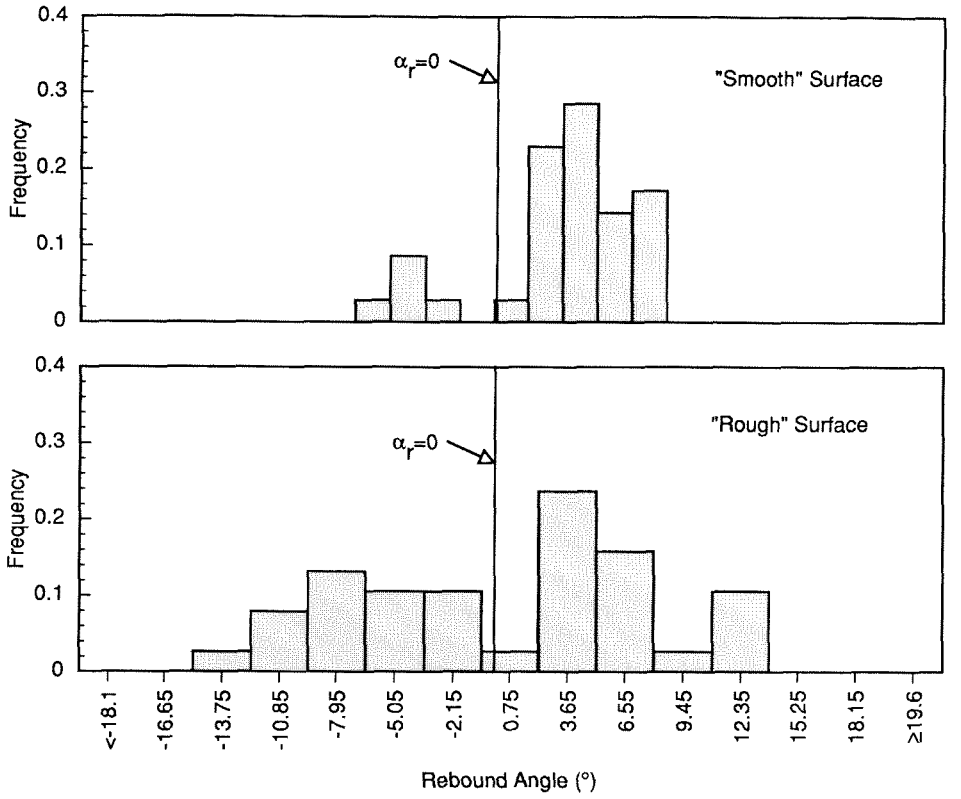


FIGURE 9. Frequency distribution of microsphere rebound angle at $\alpha_i = 90°$: (a) case 1, "smooth" surface, (b) case 3, "rough" surface.



is similar to that observed beforehand when surface roughness was varied alone. It further exemplifies how surface roughness leads to higher apparent rebound angles. Specular reflection occurs for each of the two surface cases at the higher angles of incidence ($\alpha_i \geq \sim 60°$). The middle and bottom graphs of $\mu$ and $e$ versus $\alpha_i$ show that this combined effect yields no differences beyond the measurement uncertainty at higher angles of incidence (for $\alpha_i \geq \sim 30°$). However, as the angle of incidence is decreased below $\sim 30°$, the differences between the two cases become apparent. Here, the combined effect of increased surface roughness and Hertzian stiffness at a given $\alpha_i$ is to increase the measured values of $e$ and $\mu$. The Tedlar™ surface case represents the relatively limiting case in which the measured $e$ increases to a value greater than unity, and the measured value of $\mu$ suggests that the microsphere is rolling throughout the duration of contact at an incidence angle as low as $\sim 12°$. These trends are explained according to the same arguments presented in the previous section.

The combined effect of an increase in surface roughness and Hertzian stiffness on the normalized translational kinetic energy loss versus the angle of incidence is shown in Fig. 11. The observed general trend of $T_L^*$ versus $\alpha_i$ for the two surface cases is characteristic of surface impact by rounded or blunt particles (in distinction to sharp or cutting particles). Over the incidence angle

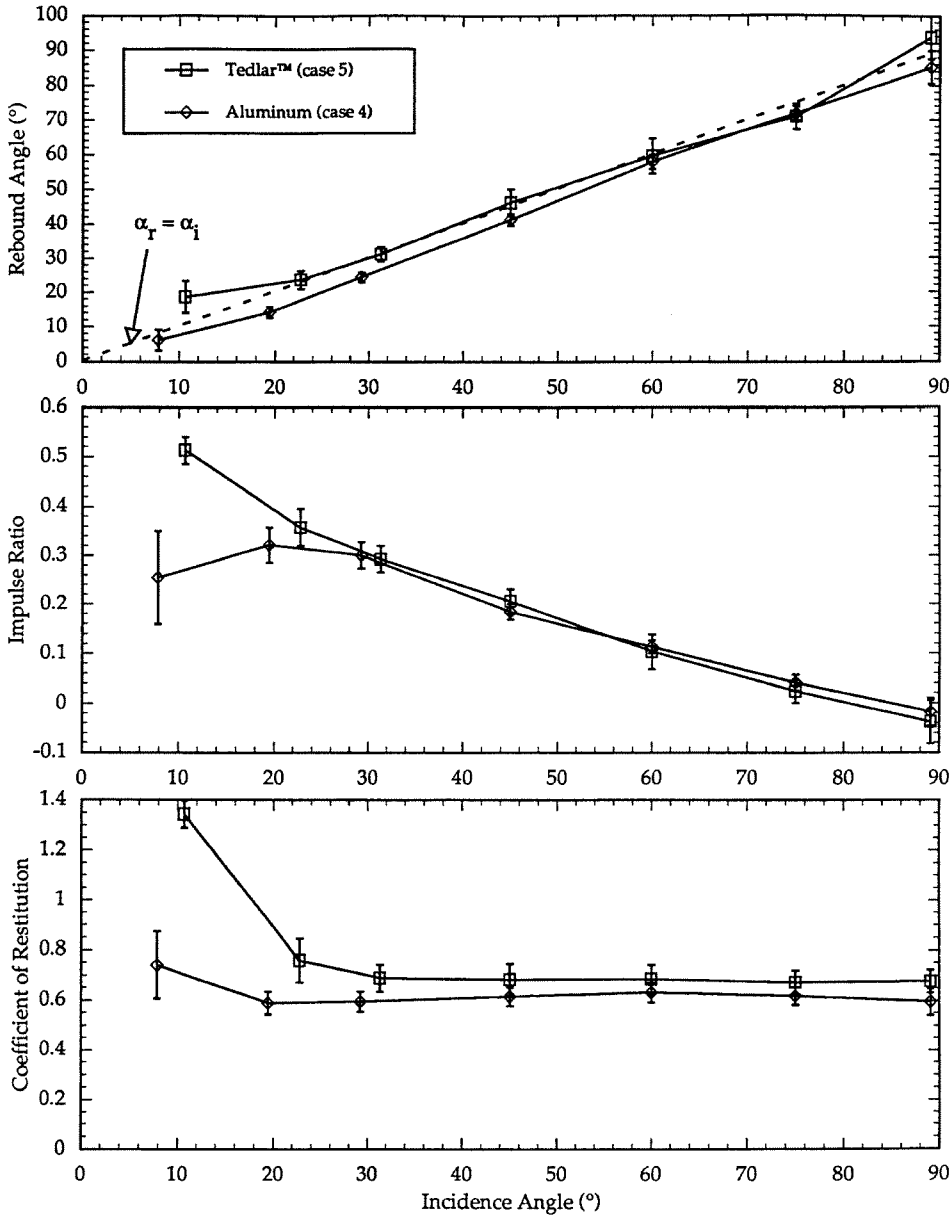


FIGURE 10. Impulse ratio, coefficient of restitution, and rebound angle versus incidence angle: comparison of aluminum (case 4) and Tedlar™ (case 5) surfaces.

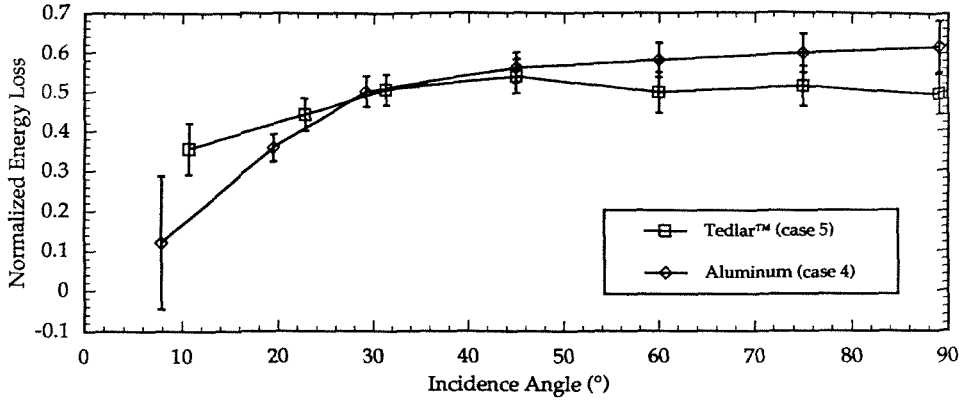


FIGURE 11. Normalized translational kinetic energy loss versus incidence angle: cases 4 and 5.



range from near 45° to 90°, $T_L^*$ is constant for each surface case to within its true mean value estimates, supporting the occurrence of specular reflection. For this incidence angle range, the normalized energy loss is greater for case 4 because the coefficient of restitution for that case is lower (recall that at $\alpha_i = 90°$, the normalized energy loss equals $1 - e^2$). At low incidence angles ($\alpha_i \leq 30°$), a greater loss in the normalized translational kinetic energy occurs with increasing surface roughness and Hertzian stiffness (case 5). This is a consequence of the relatively higher measured values of $\mu$ obtained for this case at these angles [see the middle graph of Fig. 10 and then Eq. (4)]. The physical reason for this behavior is not presently understood. The effects of surface roughness and Hertzian stiffness, however, cannot be separated because the subject experiments did not involve the variation of only one of these parameters.

### *Combined Microsphere Size and Material Effects*

The effect of a change in the microsphere size and material is illustrated best by comparing two experimental cases (5 and 6) in which the surface was the same (Tedlar™) and the microsphere size and material were different (15–65 $\mu$m diameter stainless steel and 3–13 $\mu$m diameter Ag-coated glass). In Fig. 12, $\alpha_r$, $\mu$, and $e$ are plotted versus $\alpha_i$, revealing that there are no discernible differences between the two cases to within the experimental uncertainty. The trends of the three parameters versus $\alpha_i$ are similar to those presented previously, where the combined effect of the Tedlar™ surface's roughness and Hertzian stiffness at low angles of incidence yields a nonlinear relation between $\alpha_r$ and $\alpha_i$, an increased value in the measured $e$ to greater than unity, and an increased value in the measured $\mu$. Thus, effects associated with the Tedlar™ surface itself dominate over any microsphere size or material effects.

It is also noted that no microsphere capture was observed down to normal velocity component values of 0.42 and 0.29 m/s for cases 5 and 6, respectively. These results collectively imply that the adhesion effects typically seen under normal ($\alpha_i = 90°$) incidence as the particle size is decreased are probably present at low angles of incidence, but are "masked" by variations due to the combination of tangential motion and surface roughness.

### *Electrical Charging Effects*

A subsidiary experiment was performed to examine the effect of electrical charge. In

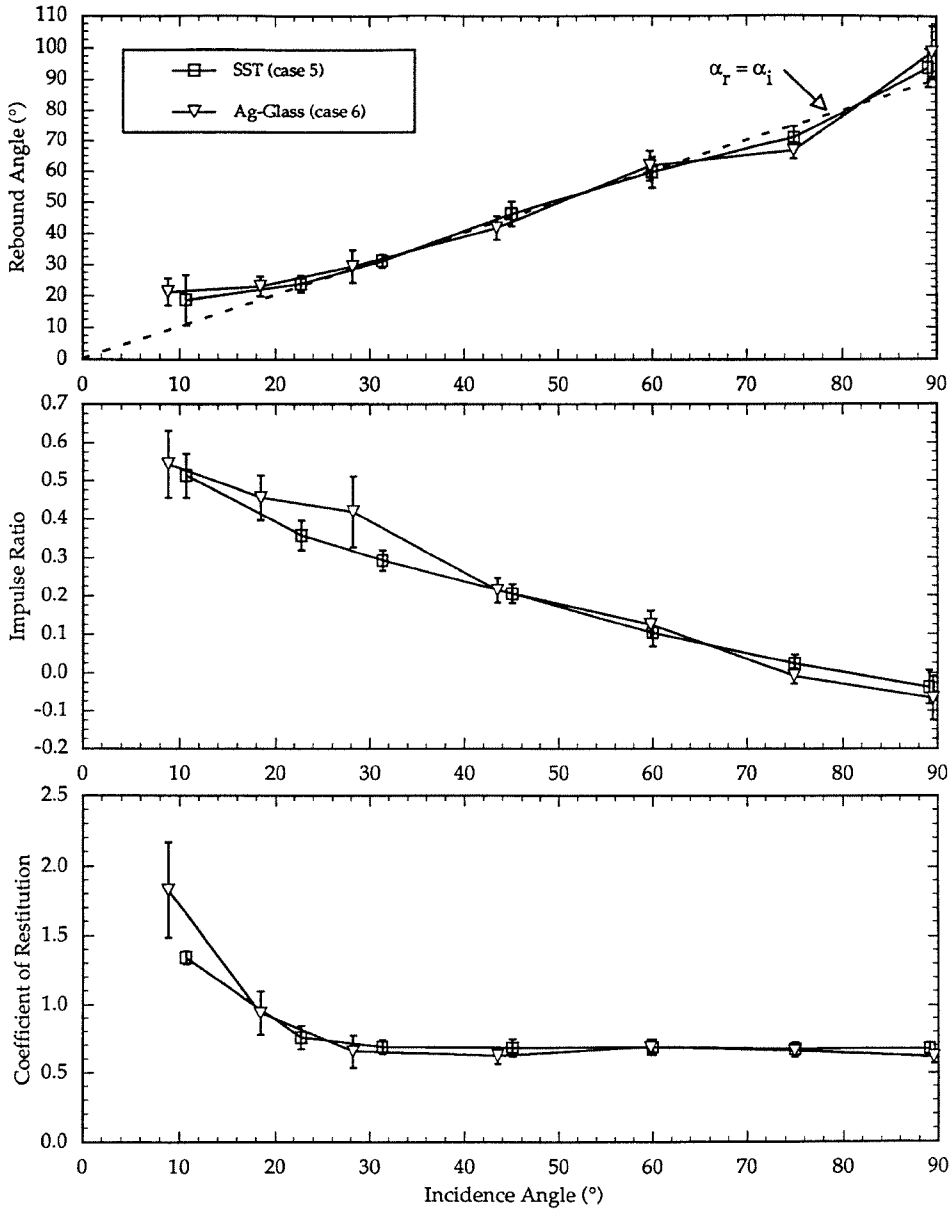


FIGURE 12. Impulse ratio, coefficient of restitution, and rebound angle versus incidence angle: comparison of stainless steel (case 5) and Ag-coated glass (case 6) microspheres.

this particular experiment, microspheres were charged by induction inside the EPD. The microsphere and surface type were the same as in the base case. Only two angles of incidence were studied ($\alpha_i = 90°$ and 10°). The apparent effect of the increase in charge (from about 1 aC [~6 elementary charges] to 50 fC [$\sim 3 \times 10^5$ elementary charges]) was a decrease in the value of $e$ at normal incidence to 0.71 from 0.79. Although relatively small, this reduction in $e$ for the charged case is most likely the result of an increase in the force of adhesion due to the electrostatic image force developed between the charged conducting microsphere and the dielectric surface (see Janson (1995) for a discussion and estimate of the magnitudes of the forces contributing to adhesion). No difference is seen in the measured values of $e$ for $\alpha_i = 10°$, where the initial normal velocity component is over 80% lower than that for normal incidence. This supports the observations of others, and from these experiments, that the effects of adhesion forces can be masked by the effects of tangential motion during oblique collisions. Finally, it is reemphasized that electrical charge effects were present only in the subsidiary experiments, and were negligible for all other experiments reported herein.



## SIMULATION

A simulation of the dynamics of a microsphere colliding at normal incidence with a massive flat surface in the presence of adhesion forces was presented by Brach and Dunn (1995). For the present study, a numerical simulation similar to the base case was followed where identical spherical particles impact the surface with the same initial total velocity, but with varying incidence from normal (90°) to shallow angles approaching 5°. Microspheres with shallow angles of incidence have a relatively small initial normal velocity and a large initial tangential velocity. The physical and initial conditions assumed for the simulation are listed in Table 2. Figures 5 and 13 show the results of this simulation. The experimental and simulation results in some ways are quite similar and follow the same trends, but there are some notable differences.

TABLE 2. Physical and Initial Conditions for Microsphere Impact Simulation.

| | |
|---|---|
| **Stainless Steel Sphere** | |
| $\rho$, density | 8000 kg/m$^3$ |
| $E$, Young's Modulus | 190 GPa |
| $\nu$, Poisson's ratio | 0.27 |
| $d$, diameter | 70 $\mu$m |
| $m$, mass | $14.37 \times 10^{-10}$ kg |
| $k$, radius of gyration | 22.14 $\mu$m |
| $SiO_2$ Surface | |
| $\rho$, density | 2330 kg/m$^3$ |
| $E$, Young's Modulus | 130 GPa |
| $\nu$, Poisson's ratio | 0.28 |
| Coefficient of Friction | 0.14 |
| Initial Conditions | |
| $\alpha_i$, angle of incidence | $90° \rightarrow 0°$ |
| $v_n$, initial normal velocity | 1.75 sin $\alpha_i$, m/s |
| $v_t$, initial tangential velocity | 1.75 cos $\alpha_i$, m/s |
| $\omega$, initial angular velocoty | 0 rad/s |

To "calibrate" the simulation, two damping coefficients must be chosen (see Brach and Dunn, 1995). For this study, this was done by matching the coefficient of restitution of the simulation at $\alpha_i = 90°$ and $\alpha_i \sim 9°$ to those of the data. The simulation results in Fig. 13 show that the coefficient of restitution drops suddenly at small angles of incidence, reflecting the presence of adhesion. For this particular simulation, lower angles of incidence have lower initial normal velocities. From the simulation, the effect of adhesion grows significantly below about $\alpha_i = 20°$, whereas a more gradual drop appears at about $\alpha_i = 40°$ and below in the experiments. Attachment or capture of the microsphere due to adhesion is predicted by the simulation to occur at about $\alpha_i = 5°$, with a corresponding initial normal velocity $v_n = 0.15$ m/s. According to the simulation, this is the capture velocity whether or not $v_t$ is zero. It is not clear from the experiments if this is true.

One of the greatest differences between the simulation and experiment is for the

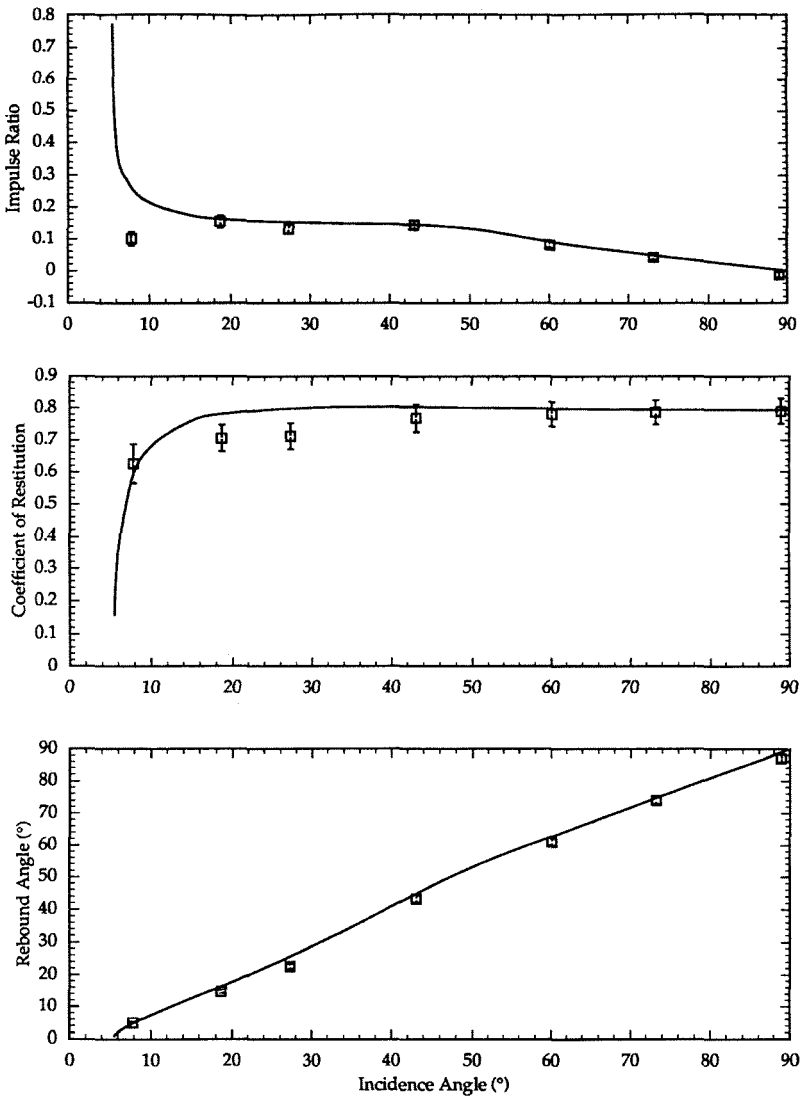


FIGURE 13. Simulation of the impulse ratio, coefficient of restitution, and rebound angle versus incidence angle (solid curves) and data from case 1.

impulse ratio at low angles of incidence. Below about 20°, the experimental impulse ratios decrease, whereas the simulation values rapidly increase. The reason for the increase in the theoretical values seems straightforward. Being an attraction force, the impulse of the adhesion force is negative (toward the surface), and at low initial normal velocities begins to overwhelm the body deformation impulse (positive, away from the surface). Consequently, the normal impulse $P_n$ approaches zero at capture. The tangential impulse $P_t$ is due to sliding friction, so the ratio $\mu = P_t/P_n$ grows as $\alpha_i$

decreases. Additional low speed and low incidence angle oblique impact data are necessary to confirm or reject the trend shown by the simulation.

The rebound angles are close to the incident angles for both the experimental data and the simulation, as seen in the lower part of Fig. 4. Figure 5 shows that the normalized kinetic energy loss increases from grazing incidence toward its highest levels of $\sim 0.40$, and then levels off toward normal incidence. Except at low and high angles, the normalized energy loss from the simulation shown in the figure (solid curve) is seen to lie considerably below the experimental values. The simulation accounts for the rotational motion of the microspheres, and so includes the rotational energy in the calculation of the normalized energy loss. On the other hand, the experimental values are based on translational velocities only. The normalized energy loss without including the final rotational energy was also calculated from the simulation and is plotted in Fig. 5 (dotted curve). It agrees quite well with the data, and implies that the lower normalized energy loss from the simulation is not an inadequacy in the model, but is due to the unmeasured rotational energy. To confirm this, consider the following. If the particle is rolling when it leaves the surface, then the final kinetic energy is $(1/2)mV_n^2 + (1/2)mV_t^2 + (1/2)mk^2\Omega^2 = (1/2)mV_n^2 + (1/2)m(1 + 2/5)V_t^2$ since $V_t = r\Omega$ for rolling and $k^2/r^2 = 2/5$ for a sphere. Thus, spin at rebound contributes a significant amount of kinetic energy except at normal incidence (when $V_t$ is small) and at grazing incidence (where the condition of rolling does not apply and $\mu \ll \mu_c$).

## CONCLUSIONS

The present experiments have confirmed at the individual impact-event level several findings and assertions of previous investigators, and have provided new, detailed information on particle impact behavior at oblique incidence.

The microspheres in the experiments did not show the propensity for capture at the same low initial normal velocities as indicated by the simulation. This could mean that the values of the coefficients of the force terms used in the simulation did not correspond as closely as they should to the physical and experimental conditions or that the modeling of the tangential and normal stresses in the simulation needs improvement. This can be resolved with further experiments, particularly in the region of particle capture, and further underscores the need for fundamental measurements of dynamic contact forces at the molecular level. The lack of particle capture at low initial normal velocities also implies that high initial particle angular velocities can hinder capture. Such an effect may not be present experiments in which particles are dispersed by aerosol generators into air, where angular velocities would not be high.

Variations in the measured values of the coefficient of restitution with incidence angle revealed an additional complication of the oblique impact process related to surface roughness. As expected, for the case of a molecular-smooth surface, the coefficient of restitution decreased at shallow angles of incidence because of a simultaneous decrease in the initial normal velocity. Surface roughness significantly biases the experimental measurements, yielding unrealistically high values of the coefficient of restitution at these lower angles.

Four regions of microsphere surface-contact mechanics were identified through examination of the microsphere's tangential impulse response over the full range of incidence angles. The extent of each of these regions depends on whether or not the microsphere is rolling or sliding at the time contact ends (sliding at separation occurs when $\mu < \mu_c$). This condition, in turn, depends on the friction coefficient and the initial tangential velocity of the contact point of the microsphere. This velocity is controlled by both the microsphere's angle of incidence and its initial spin (angular velocity). The effect of microsphere spin on the surface-contact mechanics also was found to increase the spread of impulse ratio values at a particular incidence angle.

Changes in surface roughness and the particle's and surface's material properties from the base case were shown to affect the impulse response. For example, the combined effect of an increase in surface roughness and a decrease in Hertzian stiffness prevented microsphere sliding throughout contact, even at very shallow incidence angles. In general, microsphere spin and surface roughness contribute to the tangential effects present at oblique incidence, which in turn can mask the effects of adhesion at low incidence angles.

Finally, the simulation matches the measured trends reasonably well, but not with the detail that was found in prior research involving only normal impact. Until experiments actually measure the dynamic normal adhesion force and its corresponding dynamic dissipation, the simulation will continue to be based on matching the *effects* of adhesion rather than the *mechanics* of adhesion. Additional unresolved issues include the nature of the tangential contact force (friction) model and the significance of rolling dissipation. Its significance, particularly in the presence of adhesion, will remain unresolved until angular velocity changes and angular rotation can be measured directly.



*ACKNOWLEDGMENTS*

We acknowledge the support of the Electric Power Research Institute (RP8034-03, Dr. Richard Oehlberg, Project Manager) for the experimental part of this study. Professor Greg Snider and Dr. Greg Bazan of the Microelectronics Laboratory at Notre Dame provided invaluable assistance in preparing the silicon surfaces and in the scanning electron micrography and profilometry of the target surfaces. Finally, we acknowledge the conscientious review of this paper by one of its referees, who made many helpful comments.

## References

Aylor, D. E., and Ferrandino, F. J. (1985). *Atmos. Environ.* 19:803–806.

Brach, R. M., and Dunn, P. F. (1995). *Aerosol Sci. Technol.* 23:51–71.

Broom, G. P. (1979). *Filtration & Separation* 16:661–669.

Buttle, D. J., Martin, S. R., and Scruby, C. B. (1989). Harwell Laboratory Report AERE-R13711, Oxfordshire, UK, 1–30.

Caylor, M. J., Dunn, P. F., and Brach, R. M. (1992). *J. Aerosol Sci.* 23(S1):519–522.

Caylor, M. J. (1993). *The Impact of Electrically Charged Microspheres with Planar Surfaces under Vacuum Conditions*, Ph.D. Dissertation. University of Notre Dame.

Coleman, H. W., and Steele, W. G. (1989). *Experimentation and Uncertainty Analysis for Engineers*. Wiley Interscience, New York.

Cooper, D. W., Wolfe, H. L., Yeh, J. T. C., and Miller, R., (1990). *Aerosol Sci. Technol.* 13:116–123.

Dunn, P. F., Brach, R. M., and Caylor, M. J. (1995). *Aerosol Sci. Technol.* 23:80–95.

Fong, M. C., Lee, A. L., and Ma, P. T. (1995). In *Particles on Surfaces* 4: *Detection, Adhesion, and Removal* (K. L. Mittal, ed.). Marcel Dekker, New York, pp. 77–99.

Ghandhi, S. K. (1983). *VLSI Fabrication Principles: Silicon and Gallium Arsenide*. Wiley, New York.

Janson, G. G. (1995). *Refined Experiments on Microsphere Impacts with Planar Surfaces*, M.S. Thesis. University of Notre Dame.

Lifshitz, J. M., and Kolsky, H. (1964). *J. Mech. Phys. Solids* 12:35–43.

Paw U, K. T. (1983). *J. Colloid. & Inter. Sci.* 93:442–452.

Shaffer, F., Massah, H., Sinclair, J., and Shahnam, M. (1994). In *Proceedings of the First International Particle Technology Forum, Part II*, American Institute of Chemical Engineers, pp. 499–504.

Sze, S. M. (1983). *VLSI Technology*. McGraw-Hill, New York.

Tabakoff, W., and Malak, M. F. (1987). *J. Turbomachinery* 109:535–540.

Wang, H. C., and John, W. (1988). In *Particles on Surfaces* 1: *Detection, Adhesion, and Removal* (K. L. Mittal, ed.) Plenum, New York, pp. 211–224.

Received December 6, 1995.